ORIGINAL ARTICLE

Mechanisms Accounting for the Formation of the Strong Winds that Caused the Tripping Incident of Transmission Line in Eastern Inner Mongolia

Shuanglong Jin[1] · Xiaolin Liu[1] · Wang Bo[1] · Zongpeng Song[1]

Abstract

Meteorological disasters pose a serious threat to the State Grid Corporation of China, which covers ~ 88% of Chinese national territory. Of these, strong winds deserve a special attention, as they often induce windage yaw discharge of transmission lines and even toppling of transmission towers, resulting in serious economic losses. On 28 June 2023, a severe tripping incident of transmission line appears in Eastern Inner Mongolia due to strong winds. In this study, we conduct comprehensive analyses to clarify the favorable background conditions and governing mechanisms for producing the strong winds. Main results are shown as follows. Synoptic analysis indicates that, the favorable background environments for the event are characterized by a strong upper-level jet associated upper tropospheric divergence; an intense middle-level warm advection ahead of a shortwave trough; and a long-lived lower-tropospheric mesoscale vortex. The strong winds that cause the tripping incident mainly occur in the southeastern quadrant of the vortex. Vorticity budget presents that the period from the mesoscale-vortex's formation to 4 h before is crucial to the mesoscale vortex, as cyclonic vorticity increases rapidly mainly due to the lower-level convergence-related vertical stretching. In contrast, the horizontal transport mainly results in a net export of cyclonic vorticity, which is the most detrimental factor. Kinetic energy (KE) budget shows that, after the mesoscale vortex forms, the strong winds within its southeastern quadrant enhance rapidly. Overall, the positive work done by the pressure gradient force associated with the mesoscale vortex dominates the enhancement of strong winds; the horizontal transport of KE is the second dominant factor, and the vertical transport of KE (i.e., the downward momentum transportation) shows the least contribution.

Keywords Strong wind · Mesoscale vortex · Kinetic energy · Vorticity budget · State grid

1 Introduction

State Grid Corporation of China (SGCC) is one of the largest power companies in the world. The SGCC covers 26 provinces (~ 88% of Chinese national territory), serving more than 1.3 billion people. It has nearly 3000 high-voltage transmission network power stations and over 1.5 million kilometers of transmission lines (Fu et al. 2020; Sun et al. 2011). Every year, the SGCC is hit by serious natural disasters, which result

✉ Shuanglong Jin
  jinshuanglong@epri.sgcc.com.cn

✉ Xiaolin Liu
  liuxiaolin@epri.sgcc.com.cn

[1] National Key Laboratory of Renewable Energy Grid-Integration, China Electric Power Research Institute, Beijing 100192, China

in great economic losses. Of the power grid faults, more than 40% are due to natural disasters (Sun et al. 2011), with the meteorological disasters contributing the most. This situation is worsening as severe weathers show a notable increase in their intensity and frequency under a warming global climate (Fu et al. 2016; Li et al. 2016; Song et al. 2019; Sun et al. 2019). Among the meteorological disasters (e.g., rainstorms, windstorms, lighting, blizzard, freezing rain, etc.), the windstorms usually pose a serious threat to the transmission lines (Fu et al. 2020; Xie and Li 2006; Yang et al. 2009). The damages caused by strong winds to the power facilities mainly include windage yaw discharge of transmission lines, wire breakages, substation-equipment destruction, and even tower collapses (Zhang et al. 2015, 2019; Cevik et al. 2019; Li et al. 2023). For instance, on 14 May 2021, strong winds associated with a downburst event in Zhejiang Province caused six 500-kilovolt (kV) transmission line towers to topple down, resulting in a large range of power outages. On 15 April

Korean Meteorological Society ∅ Springer

2023, strong winds associated with a cold front occurred in Shanxi Province, and caused the shutdown of five high-voltage transmission lines (including 220 kV and above). This resulted in serious economic losses in Shanxi Province. Both the 200-kV and 500-kV transmission lines belong to the high-voltage transmission line, which play an important role in transmitting and distributing electric energy among the power facilities of the SGCC.

On 28 June 2023, a severe tripping incident of transmission line appeared in Eastern Inner Mongolia due to strong winds, during which a total of 9 power transmission lines of 66 kilovolt and above (including 550 kV) tripped. This resulted in closing down of some power plants and a widespread power outage in Eastern Inner Mongolia, which caused serious economic losses. According to previous studies, strong winds during warm seasons (from May to September) were mainly associated with squall lines, supercell storms, mesoscale vortices, extratropical cyclones, shortwave troughs, low-level jets, and typhoons (Fu et al. 2020; Zhang et al. 2019; Li et al. 2023; Markowski and Richardson 2010; Yang and Sun 2014). In addition, the orographic effects also played an important role in generating strong winds, mainly through producing gravity waves (Lu et al. 2014), inducing downslope winds (Zhang et al. 2018), increasing horizontal pressure gradient (Ding et al. 2019), and exerting a narrow pipe impact (Wang et al. 2011). To the best of our knowledge, thus far, there were few studies that investigated the mechanisms governing the formation of strong winds in Eastern Inner Mongolia. This increases the difficulty for accurately predicting such type of events. Overall, a deeper understanding of the key mechanisms dominating the formation of the strong winds would ensure a more reliable guarantee service for the safe operation of the SGCC in Eastern Inner Mongolia. To this end, the primary purpose of this study is to (i) clarify the favorable background conditions for the strong winds, and to (ii) determine the governing mechanisms for producing the strong winds that caused the tripping incident of transmission line in Eastern Inner Mongolia on 28 June 2023. The remainder of the article is designed as the following shows. Section 2 presents the data used and the diagnosis methods; Section 3 analyzes the background conditions for the event; Section 4 shows the diagnosis results; and Section 5 provides a conclusion and discussion.

2 Data and Method

2.1 Data

In this study, a total of two types of data were used: (i) the 30-min, $0.1° \times 0.1°$ Global Precipitation Measurement (GPM) IMERG precipitation data (Huffman et al. 2019) was used to analyze the precipitation features; and (ii) the hourly,

$0.25° \times 0.25°$ ERA5 reanalysis data (including zonal wind, meridional wind, vertical wind, temperature, geopotential height) at 37 pressure levels (Hersbach et al. 2020), and surface (e.g., mean sea level pressure, 10-m wind) were utilized for synoptic analyses and diagnoses.

2.2 Diagnosis Methods

In order to understand the formation mechanisms of the strong winds that caused the tripping incident of transmission line in Eastern Inner Mongolia, we calculated the kinetic energy (KE) budget, as KE is a direct indicator for the wind speed (Fu et al. 2013). The KE budget equation developed by Ma et al. (Ma et al. 2023) was used in this study. Its expression is as follow shows:

$$\frac{\partial k_h}{\partial t} = -u\frac{\partial k_h}{\partial x} - v\frac{\partial k_h}{\partial y} - \omega\frac{\partial k_h}{\partial p} - u\frac{\partial \Phi}{\partial x} - v\frac{\partial \Phi}{\partial y} + WF, \quad (1)$$

where $k_h = (u^2 + v^2)/2$ represents the KE of the horizontal wind (u and v are the zonal and meridional wind, respectively; and the subscript 'h' denotes the horizontal component); t stands for the time; ω stands for the vertical velocity in the pressure coordinate; p is the pressure; Φ is the geopotential; f denotes the Coriolis parameter; and WF stand for the work done by the horizontal friction force.

Term $\frac{\partial k_h}{\partial t}$ is the local temporal derivative of KE (LTK); $-u\frac{\partial k_h}{\partial x} - v\frac{\partial k_h}{\partial y}$ stands for the horizontal advection of KE (HAK), $-u\frac{\partial k_h}{\partial x}$ and $-v\frac{\partial k_h}{\partial y}$ are defined as HAK_U and HAK_V, respectively; $-\omega\frac{\partial k_h}{\partial p}$ represents the vertical advection of KE (VAK); $-u\frac{\partial \Phi}{\partial x} - v\frac{\partial \Phi}{\partial y}$ denotes the work of pressure gradient force (WPF), and $-u\frac{\partial \Phi}{\partial x}$ and $-v\frac{\partial \Phi}{\partial y}$ are defined as WPF_U and WPF_V, respectively. We defined TOT=HAK+VAK+WPF, which represents the total effect of all terms on the right-hand side of the Eq. (1) except for the friction force.

In this event, there was a mesoscale vortex (Fu et al. 2020) which was directly related to the strong winds. Thus, we used the vorticity budget equation to understand the evolutionary mechanisms of the vortex. According to previous studies (Holton 2004; Fu et al. 2017, 2019), the area mean vorticity can be used as an effective indicator for a mesoscale vortex. The vorticity budget equation has the expression as the following shows.

$$\frac{\partial \zeta}{\partial t} = -(\zeta + f)\nabla_h \cdot \mathbf{V}_h + \mathbf{k} \cdot \left(\frac{\partial \mathbf{V}_h}{\partial p} \times \nabla_h \omega\right) - \mathbf{V}_h \cdot \nabla_h \zeta - \omega\frac{\partial \zeta}{\partial p} - \beta v, \quad (2)$$

where ζ is the relative vorticity in the zenith direction (vorticity, hereinafter the same); $\nabla_h = \frac{\partial}{\partial x}\mathbf{i} + \frac{\partial}{\partial y}\mathbf{j}$ ($\mathbf{i}$ and $\mathbf{j}$ are the unit vectors in the zonal and meridional directions, respectively); $\mathbf{V}_h = u\mathbf{i} + v\mathbf{j}$ is the vector of the horizontal wind; and $\beta = \frac{\partial f}{\partial y}$.
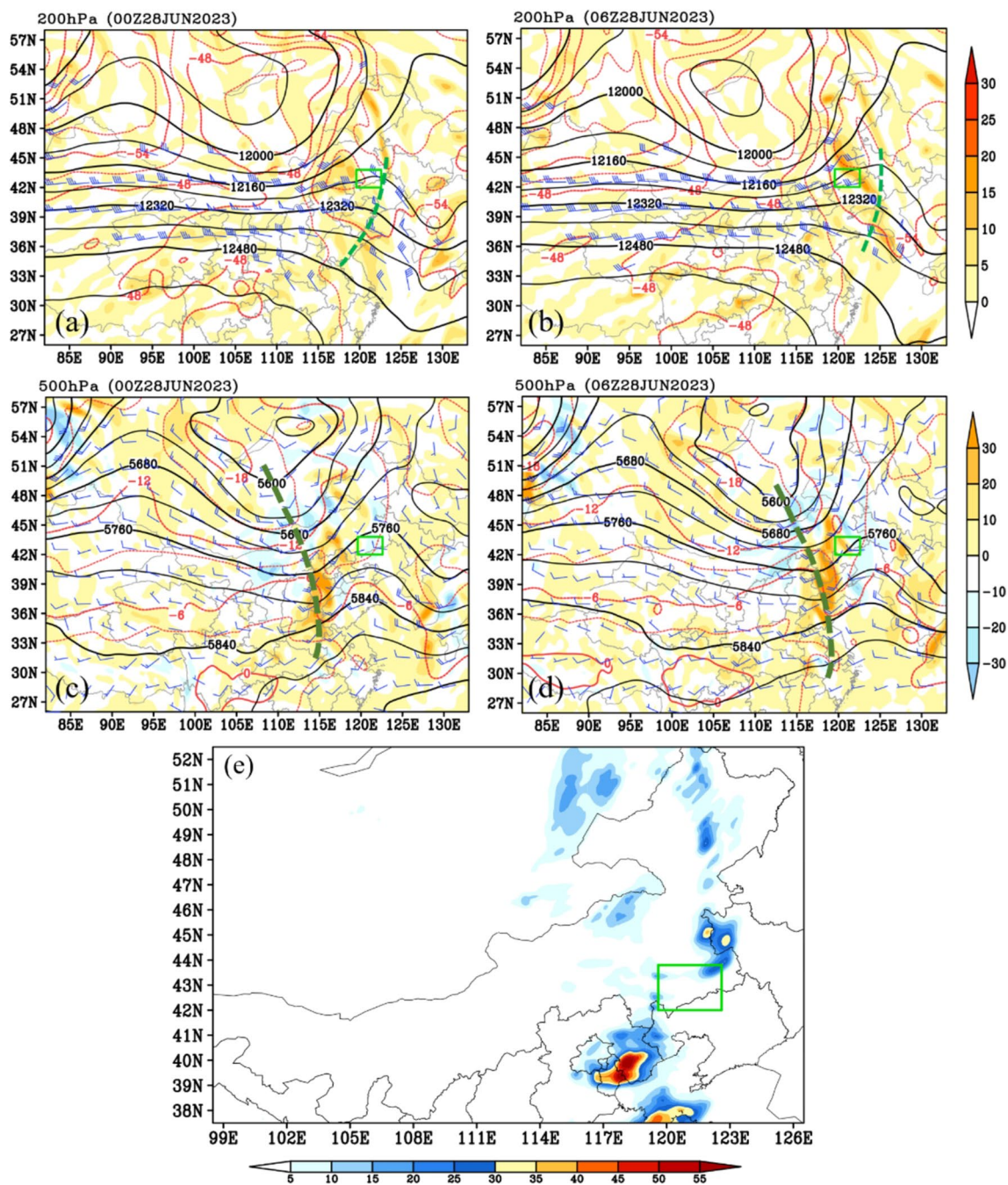
Fig. 1 Panels (**a-b**) show the geopotential height (black contour; gpm), temperature (red contour; gpm), divergence (shading; 10^{-5} s^{-1}) and wind above 30 m s^{-1} at 200 hPa (a full bar represents 10 m s^{-1}), where the green dashed lines are the ridge lines and the green boxes mark the locations where the tripping incident of transmission line appeared. Panels (**c-d**) show the geopotential height (black contour; gpm), temperature (red contour; gpm), temperature advection (shading; 10^{-5} K s^{-1}) and wind at 500 hPa (a full bar represents 10 m s^{-1}), where the green dashed lines are the trough lines. Panel (**e**) shows the accumulated precipitation (shading; mm) from 0000 to 1200 UTC 28 June, 2023

Term $\frac{\partial \zeta}{\partial t}$ is the local temporal derivative of vorticity (LTV); term $-(\zeta + f)\nabla_h \cdot \boldsymbol{V}_h$ denotes the stretching effect (STR); term $\mathbf{k} \cdot \left(\frac{\partial \mathbf{V}_h}{\partial p} \times \nabla_h \omega\right)$ represents the tilting effect (TIL); $-\boldsymbol{V}_h \cdot \nabla_h \zeta$ is the horizontal advection of vorticity (HAV); term $-\omega \frac{\partial \zeta}{\partial p}$ is the vertical advection of vorticity (VAV); term $-\beta v$ denotes the advection of planetary vorticity (APV), which is much smaller than the other terms (Fu et al. 2017, 2019). In order to represent the sum effect of all the terms on the right-hand side of Eq. (2), we defined SUM = STR + TIL + HAV + VAV + APV.
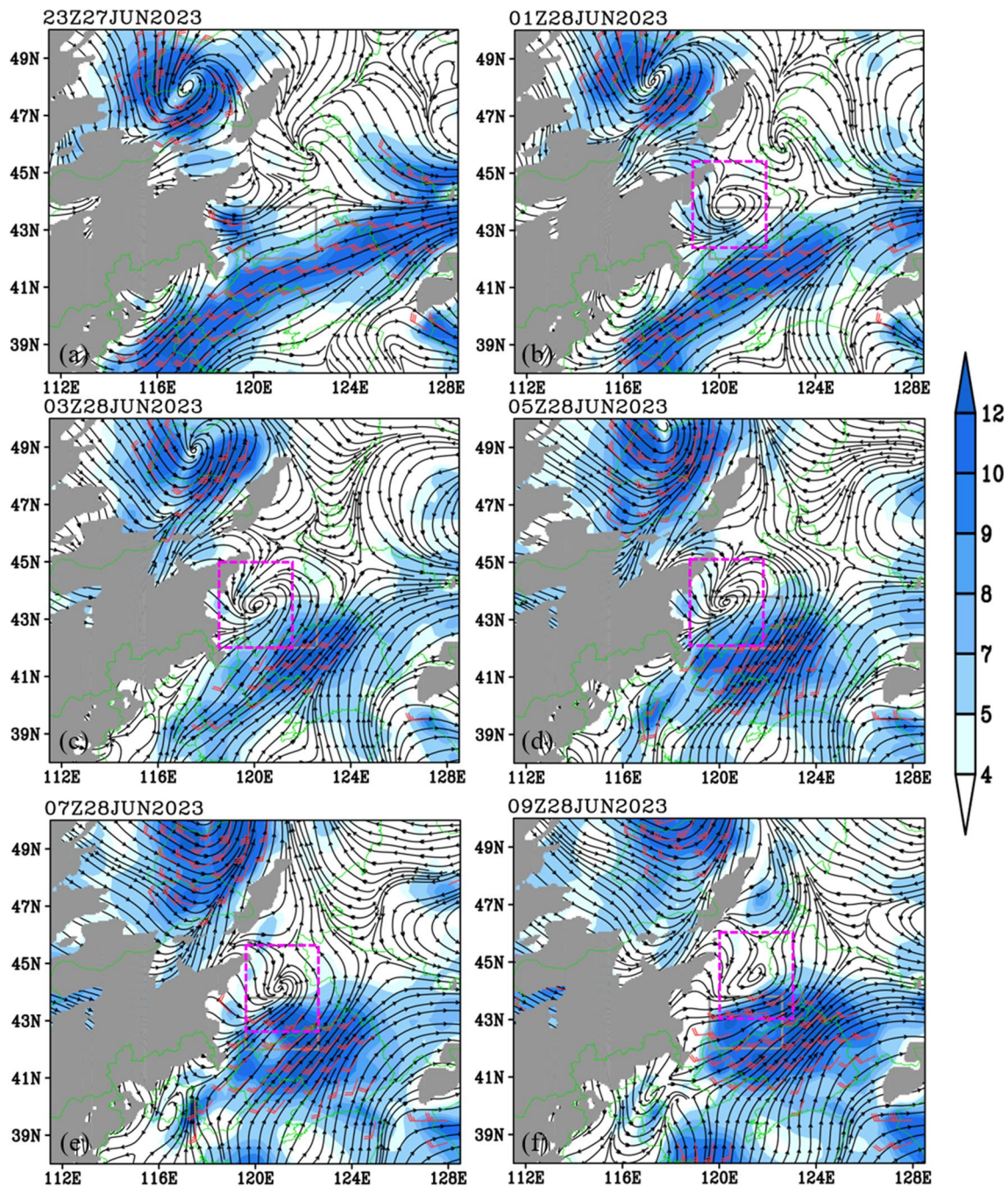
Fig. 2 Stream field (black lines with vectors), horizontal wind speed (shading; m s^{-1}), and wind above 8 m s^{-1} (a full bar represents 4 m s^{-1}) at 900 hPa, where the grey box marks the location where the tripping incident of transmission line appeared, and the purple dashed boxes outline the main body of the vortex

3 Synoptic Analyses

3.1 Background Environment

The strong winds that caused the severe tripping incident of transmission line mainly appeared during the period from 0600 to 0700 UTC 28 June 2023. The tripping incident occurred within the region of 42–43.8 °N, 119.6–122.6 °E (as the green boxes in Fig. 1 show), which was defined as the key area of the event. From Fig. 1a-b, it can be seen that, before the strong winds appeared within the key region, the Eastern Inner Mongolia was mainly controlled by the western section of a high-pressure ridge. The key area was located beneath an intense upper-level divergence that was
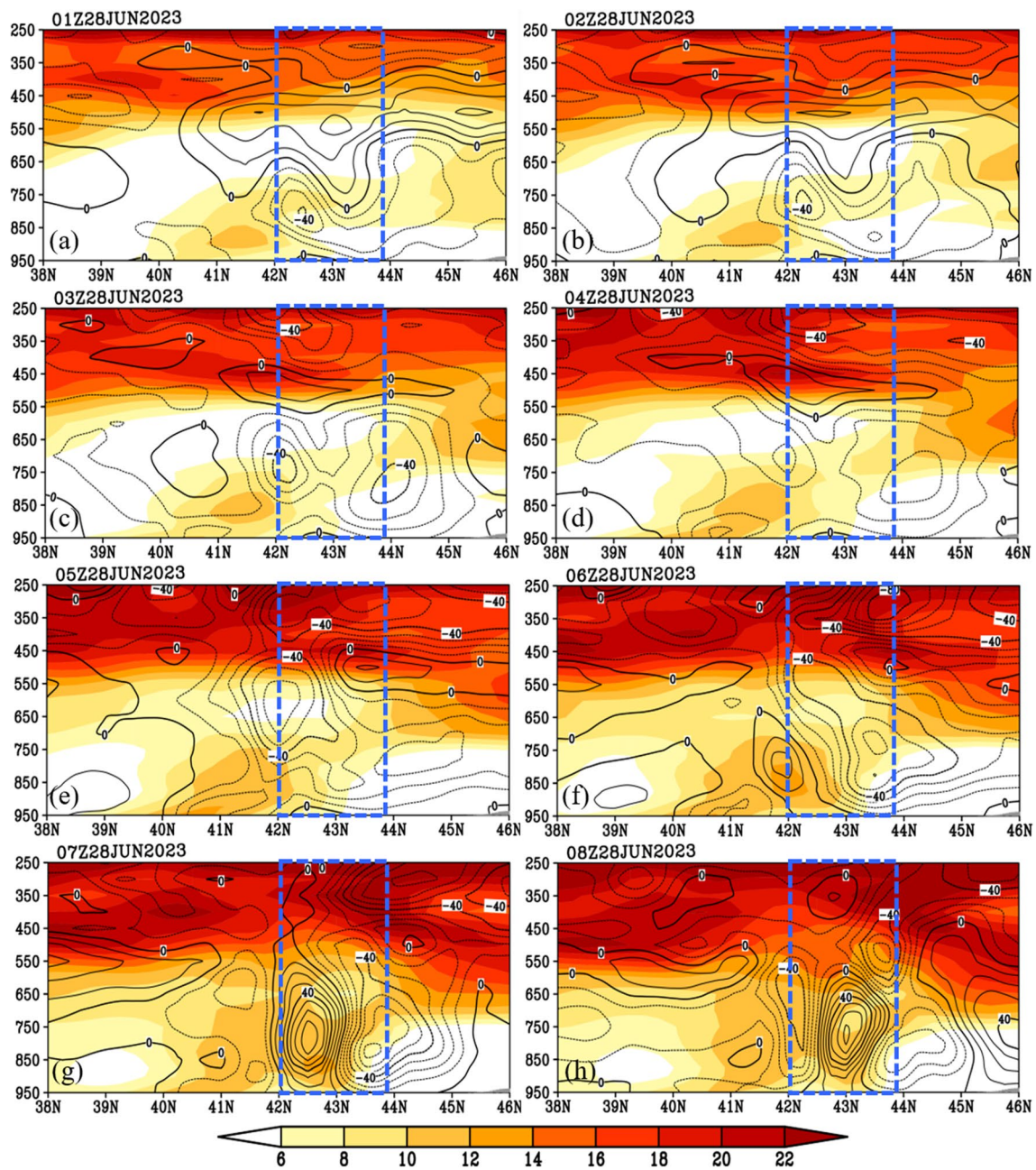
Fig. 3 Zonally averaged (from 119.5 °E to 122.5 °E) horizontal wind speed (shading; m s^{-1}), and vertical velocity (black contours; 10^{-2} Pa s^{-1}), where grey shading shows the zonally averaged terrain, and the blue dashed boxes show where the tripping incident of transmission line appeared

associated with a strong upper-level jet. This condition was favorable for the development of ascending motions due to the fluid continuity (Markowski and Richardson 2010). In the middle troposphere, the western Pacific subtropical high was relatively weak, which was mainly located at lower latitudes. The key region was located ahead of a shortwave trough (Fig. 1c-d), where there was a notable warm advection. According to the quasi-geostrophic theory, warm advection contributed to promote ascending motions (Holton

2004). Due to the favorable conditions discussed above, precipitation occurred within the key region (Fig. 1e).

3.2 Evolution of the Mesoscale Vortex

The most striking feature of the event was that a mesoscale vortex appeared at 900 hPa (Fig. 2), which was directly related to the strong winds. In this study, we used the definition from Fu et al. (Fu et al. 2022) to define a

Fig. 4 Panel (**a**) shows the region averaged (within the vortex's main body) vorticity budget results (10^{-10} s^{-2}), where the thick grey dashed line marks the time when the key-region averaged vorticity began to grow, and the thin grey dashed line is the zero line. Panel (**b**) shows the region averaged (within the vortex's main body) vorticity (black line; 10^{-5} s^{-1}), vertical velocity (red line; cm s^{-1}) and divergence (blue line; 10^{-5} s^{-1}), where the thick grey dashed line marks the time when the key-region averaged vorticity began to grow, and the thin grey dashed line is the zero line
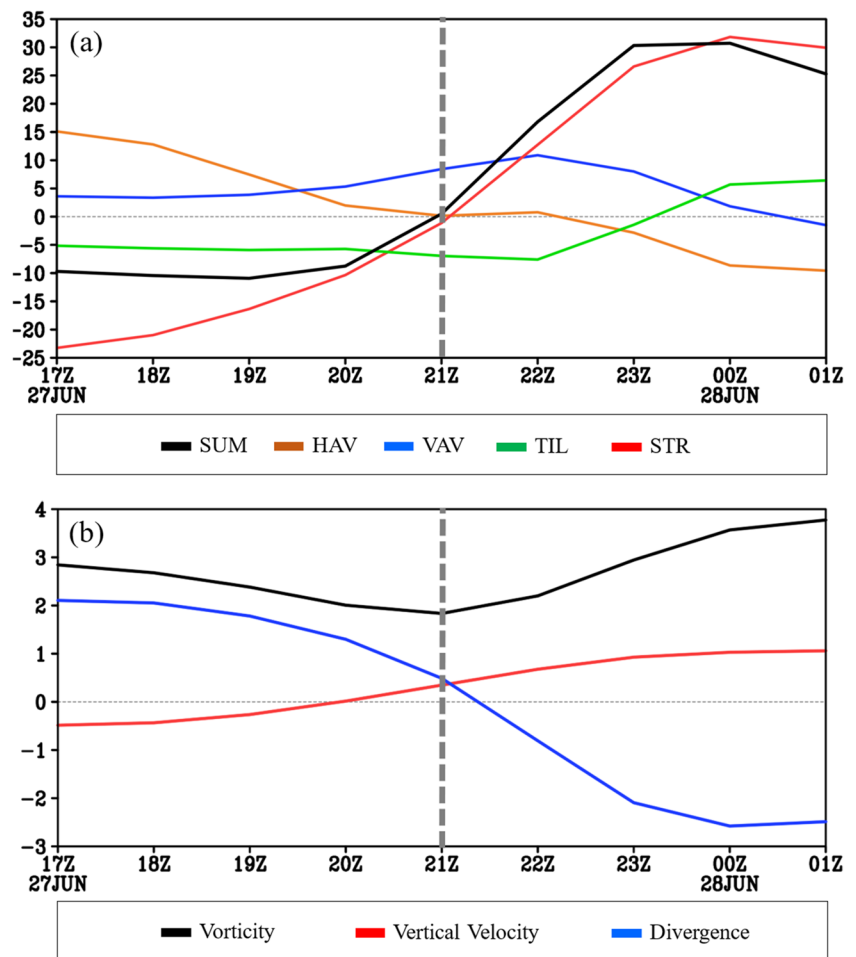
mesoscale vortex. It contains two conditions: (i) a closed counterclockwise circulation in the stream field; and (ii) a notable cyclonic-vorticity center (vorticity $\geq 10^{-5}$ s^{-1}). As Fig. 2a shows, two hours before the formation of the vortex, a cyclonic shear line appeared to the northwest of the key region, and in the meanwhile, a southwest-northeast stretching low-level jet appeared in the regions southwest, south and east of the key region. At 0100 UTC 28 June 2023, the mesoscale vortex formed, with its center located northwest of the key region. In this stage, the southwest-northeast stretching low-level jet weakened, particularly for the section east of the key region (Fig. 2b). From 0100 to 0500 UTC 28 June 2023, the vortex maintained a quasi-stationary behavior (Fig. 2b-d), and the wind speed southeast of the key region enhanced gradually. From 0500 to 0700 UTC 28 June 2023, the mesoscale vortex moved eastward (Fig. 2d-e), and the wind speed within the southern section of the key region increased notably. This rapid enhancement in wind speed directly accounted for the tripping incident of transmission line. After that, the mesoscale vortex kept moving eastward, and dissipated at 2000 UTC 28 June 2023. Overall,

the mesoscale vortex lasted for 19 h, with the strong winds mainly appeared in its southern section.

3.3 Vertical Features

As Fig. 3a-d show, in the earlier stage (from 0100 to 0400 UTC 28 June 2023), there was a strong wind band which maintained at the levels above 550 hPa. In the meanwhile, another relatively strong wind band maintained at the levels below 650 hPa. Between the two strong wind bands, there was a weak wind zone which was mainly located in the layer of 550–650 hPa. The weak wind zone was mainly associated with descending motions, which shrank rapidly in area with time. In this stage, the lower layer (below 650 hPa) of the key region was mainly dominated be ascending motions, and relatively strong winds mainly appeared in the southern section of the key region (the strong wind center did not enter the key region). During the later stage (from 0500 to 0700 UTC 28 June 2023), the upper-level and lower-level strong wind zones both intensified (Fig. 3e-g), and strong ascending motions appeared between the two wind zones. In this stage,
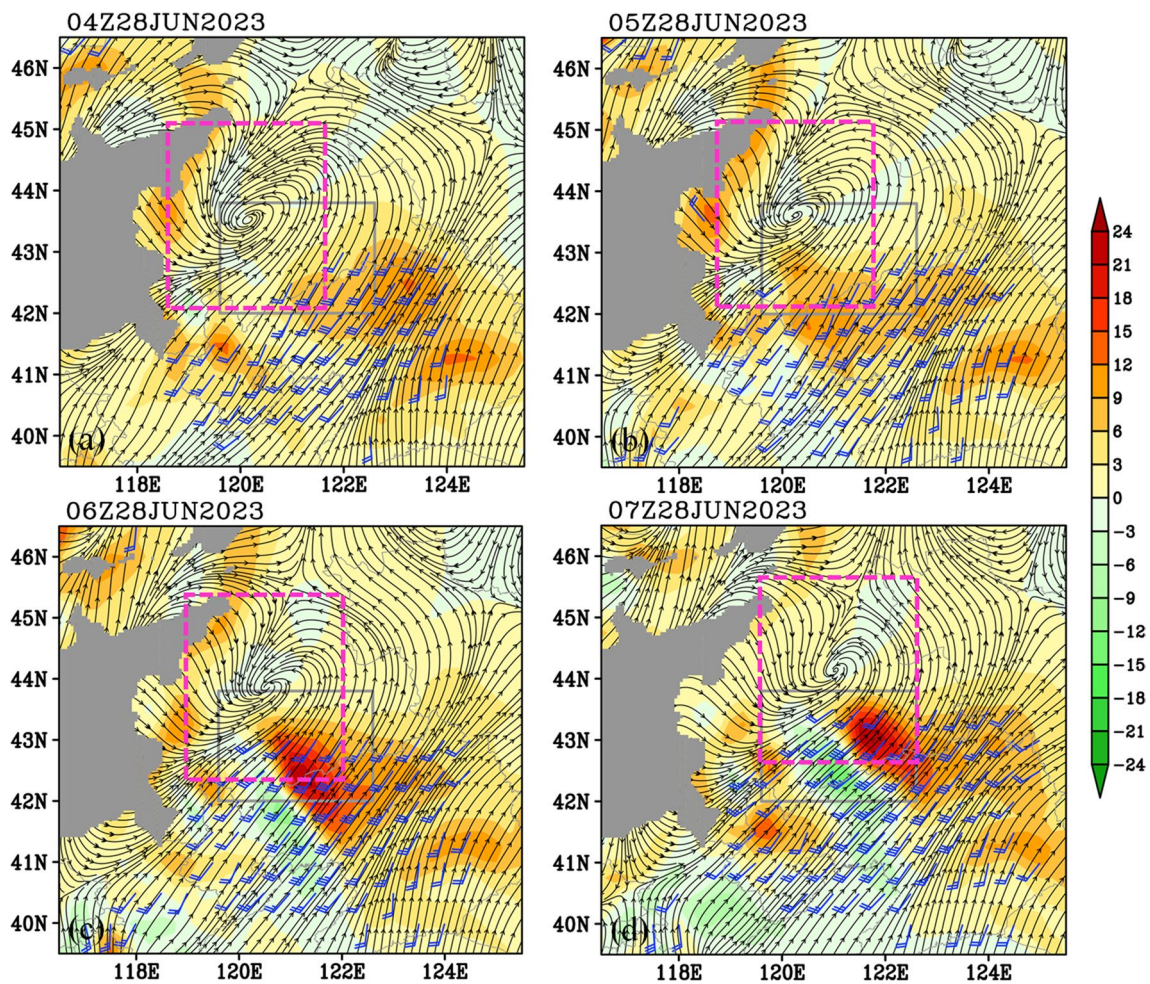
Fig. 5 The term TOT (shading; 10^{-3} W kg^{-1}), stream field (black line with arrows), and wind above 8 m s^{-1} (a full bar represents 4 m s^{-1}) at 900 hPa, where the grey box marks the location where the tripping incident of transmission line appeared, the purple dashed boxes outline the main body of the vortex, and the grey shading show the terrain above 1000 m

the lower-level strong wind zone stretched northward, with a center appeared within the key region, which corresponded to the strong winds that caused the tripping incident of transmission line. Strong descending motions developed rapidly within the key region, and in the meanwhile, ascending motions also enhanced and dominated the northern section of the key region. After that, the wind speed within the key region began to weaken (Fig. 3h), and ascending motions appeared in the western section of the key region again.

4 Quantitative Diagnostic Results

4.1 Vorticity Budget

As shown in Fig. 2b, the mesoscale vortex formed at 0100 UTC 28 June 2023. In order to understand how the vortex was generated, we outlined a calculation area which

covered the main body of the vortex (i.e., the purple dashed box in Fig. 2b), and conducted an area averaged vorticity budget within this area by using Eq. (2). A sensitivity test was conducted, which found that the calculation results were insensitive to relatively small changes to its boundary lines ($\pm 0.25°$). Therefore, the calculation results based on the calculation area were representative. Before analyses, we evaluated the balance of the vorticity budget equation by a ratio of LTV/SUM. It is shown that, the ratio was between 0.61 and 1.13, with a mean value of 0.82. Therefore, the equation was balanced well, and the results could be used for further studies.

As shown in Fig. 4a, term SUM was negative before 2100 UTC 27 June 2023, and it changed to positive after that time. This was corresponding to a decrease of cyclonic vorticity within the calculation area before 2100 UTC 27 June 2023 (Fig. 4b), and an increase after that time. In addition, ascending motions changed to positive and developed after
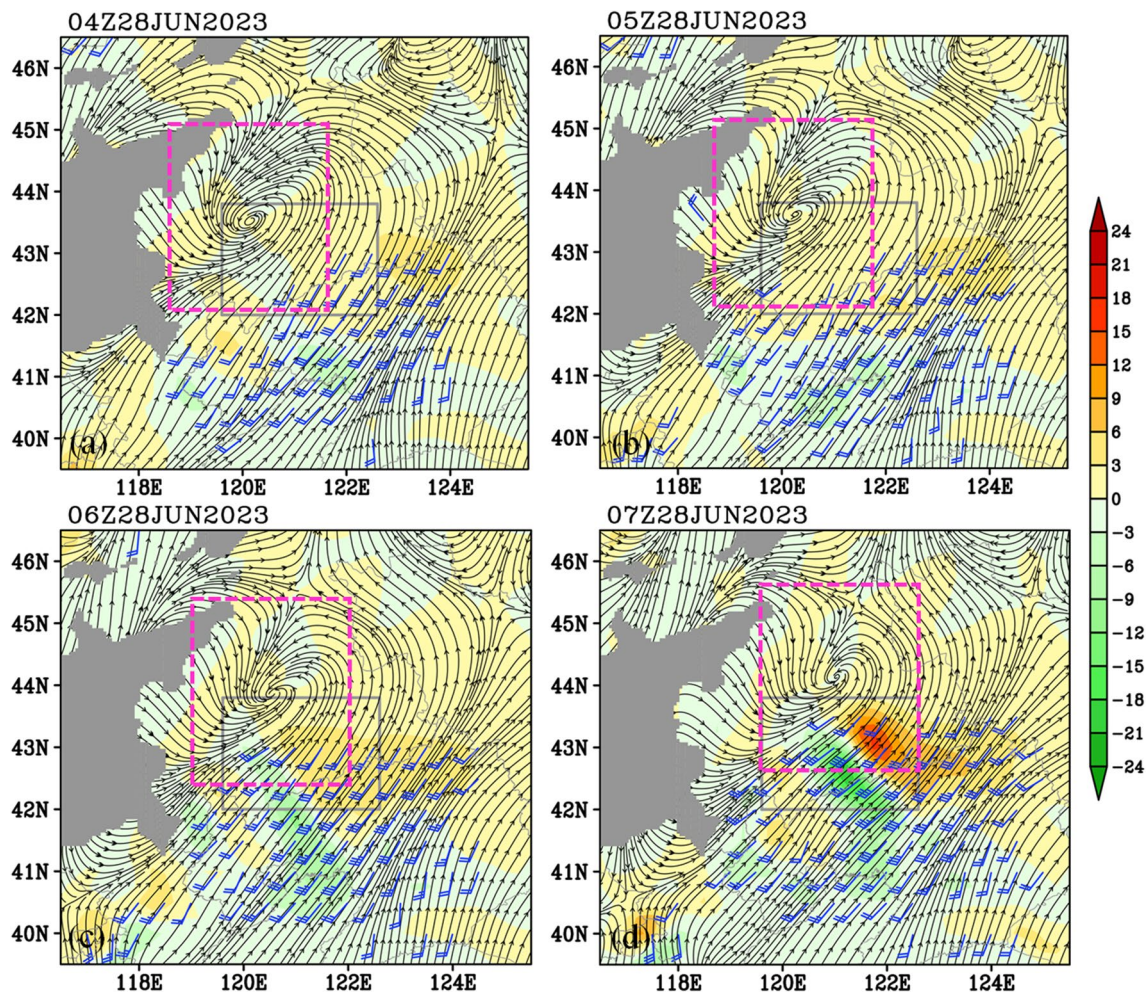
Fig. 6 The term HAK (shading; 10^{-3} W kg^{-1}), stream field (black line with arrows), and wind above 8 m s^{-1} (a full bar represents 4 m s^{-1}) at 900 hPa, where the grey box marks the location where the tripping incident of transmission line appeared, the purple dashed boxes outline the main body of the vortex, and the grey shading show the terrain above 1000 m

2100 UTC 27 June 2023. Thus, it can be concluded that, the period from 2100 UTC 27 to 0100 UTC 28 June 2023 was the key stage for the formation of the mesoscale vortex. Before 2100 UTC 27 June 2023, a strong divergence dominated the calculation area (Fig. 4b), which resulted a strong production of anticyclonic vorticity (i.e., STR; Fig. 4a). This was the dominant factor for the negative SUM. In addition, the tilting effect (i.e., TIL) also produced anticyclonic vorticity, whereas, the horizontal (i.e., HAV) and vertical transport of vorticity (i.e., VAV) mainly caused a net input of cyclonic vorticity in the calculation area, which decelerated the decrease of cyclonic vorticity. After 0100 UTC 28 June 2023, a strong convergence appeared and maintained within the calculation area (Fig. 4b), which resulted in a strong STR (Fig. 4a). This dominated the increase of cyclonic vorticity.

In the meanwhile, ascending motions developed (Fig. 4b), which enhanced the upward transport of cyclonic vorticity (i.e., VAV; Fig. 4a), and thus term VAV acted as the second dominant factor for the mesoscale-vortex's formation. In contrast, the term TIL showed an overall neutral effect, and the horizontal transport (i.e., HAV) mainly caused a net export of cyclonic vorticity from the calculation area. Therefore, term HAV was the most detrimental factor for the formation of the mesoscale vortex.

4.2 Kinetic Energy Budget

In order to understand the mechanisms governing the wind enhancement that resulted in the tripping incident of transmission line, we calculated the KE budget by using Eq. (1).
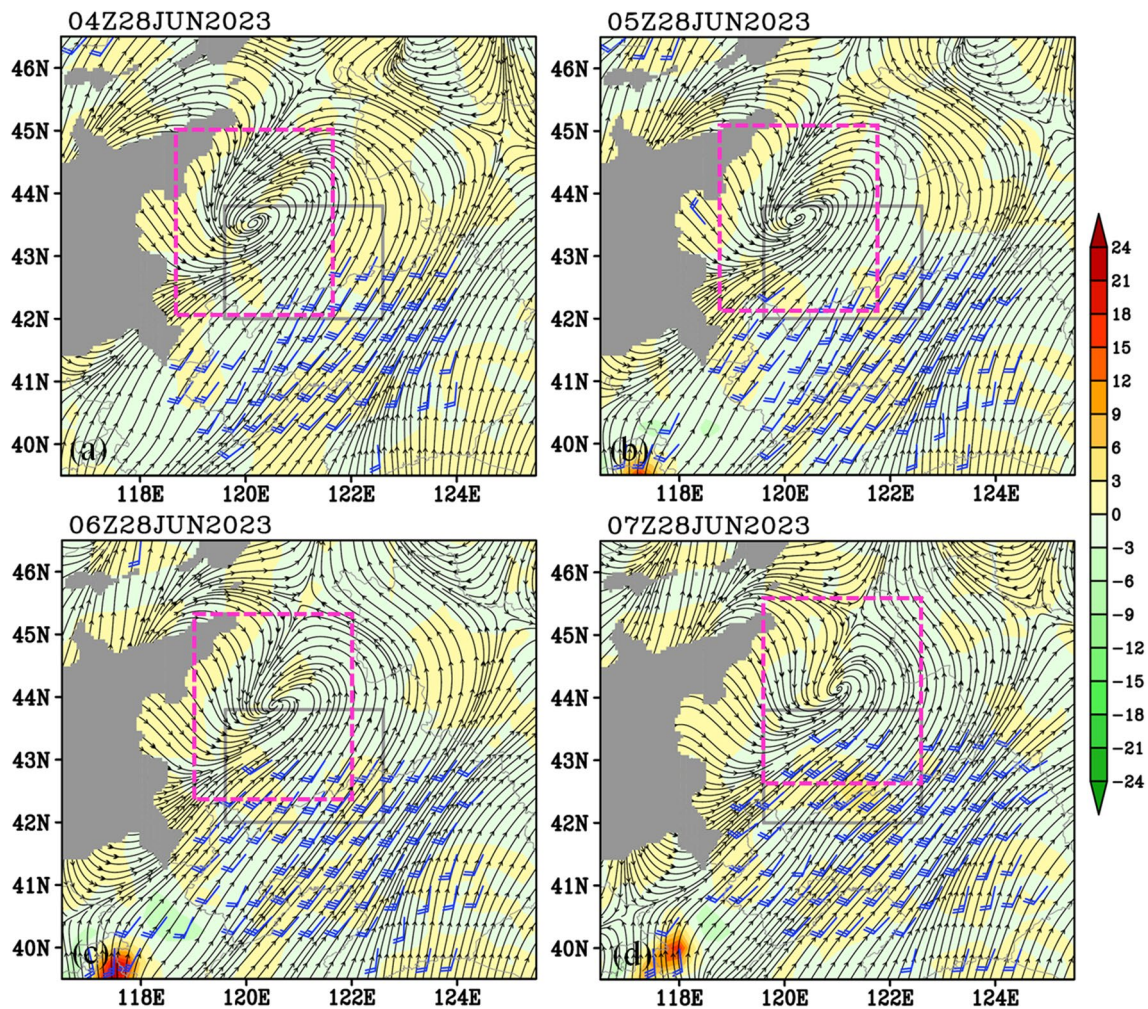
Fig. 7 The term VAK (shading; 10^{-3} W kg^{-1}), stream field (black line with arrows), and wind above 8 m s^{-1} (a full bar represents 4 m s^{-1}) at 900 hPa, where the grey box marks the location where the tripping incident of transmission line appeared, the purple dashed boxes outline the main body of the vortex, and the grey shading show the terrain above 1000 m

Similar to Sect. 4.1, before analyses, we evaluated the balance of the KE budget equation by a ratio of LTK/TOT. It was found that its mean value was ~ 0.752, implying that term TOT accounted for ~ 75.2% of the term LTK on average. Therefore, the residual effects (including friction, subgrid processes, calcualtion errors, etc.) was less important and could be ignored. As shown in Fig. 5a-b, from 0400 to 0500 UTC 28 June 2023, the key region was mainly dominated by a positive TOT term (particularly for its eastern and southern sections), implying that the KE was increasing. In this stage, the horizontal transport of KE (i.e., HAK) was relatively weak within the key region (Fig. 6a-b), since the convergence of the horizontal KE transport was relatively weak; the vertical transport of KE (i.e., VAK) was negative (Fig. 7a-b), as ascending motions transported relatively

weaker KE upward (Fig. 3d-e); and the pressure gradient force associated with the mesoscale vortex mainly did a positive work (i.e., WPG) within the key region (Fig. 8a-b). From 0600 to 0700 UTC 28 June 2023, term TOT enhanced notably in the eastern section of the key region (Fig. 5c-d), whereas, a negative center mainly maintained in the western section. This configuration means that, the horizontal wind showed a rapid increase in the eastern section, whereas, it decreased in the in the western section of the key region. From Fig. 6c-d, it is shown that, term HAK showed a negative center in the western section, and a positive center in the eastern section (Fig. 6c-d). This was consistent with the horizontal transport of KE from the western to the eastern section of the key region. In this stage, term VAK was mainly positive within the southern section of the key region
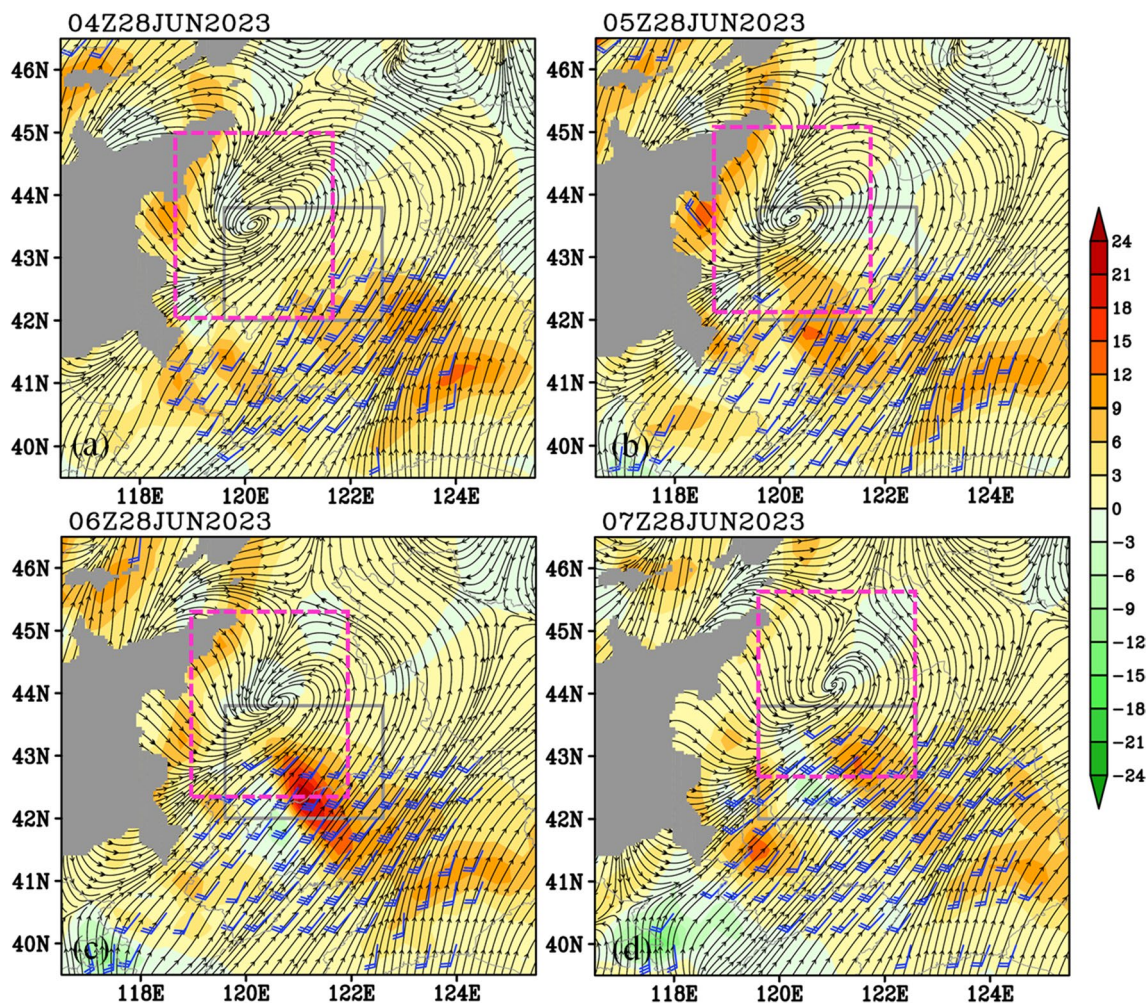
Fig. 8 The term WPF (shading; 10^{-3} W kg^{-1}), stream field (black line with arrows), and wind above 8 m s^{-1} (a full bar represents 4 m s^{-1}) at 900 hPa, where the grey box marks the location where the tripping incident of transmission line appeared, the purple dashed boxes outline the main body of the vortex, and the grey shading show the terrain above 1000 m

(Fig. 7c-d). As this region was dominated by descending motions (Fig. 3f-g), this positive VAK was mainly due to a downward momentum transportation (Fu et al. 2020). However, compared with other terms, the VAK was weaker (Figs. 7c-d and 8c-d). During this stage, the strongest term among all budget terms was the WPF. As Fig. 8c-d show, the WPF had an intense positive center in the eastern section of the key region, which was located within the southeastern quadrant of the mesoscale vortex. This was vital for producing the strong winds that caused the tripping incident of transmission line within the key region.

In order to show the overall features of the KE budget within the key region, we calculated the average of the budget results within the key region. From Fig. 9a, it can be seen that, before 0000 UTC 28 June 2023 (i.e., before the formation of the mesoscale vortex), the term TOT was negative within the key region. This indicates that the wind speed within the key region was decreasing during this period.

After the mesoscale-vortex's formation (i.e., 0100 UTC 28 June 2023), term TOT increased rapidly, with a maximum appeared in the period of 0500UTC-0700UTC 28 June 2023, during which the strong winds caused the tripping incident of transmission line. Therefore, the tripping incident was directly related to the increase of wind speed associated with the mesoscale vortex. During the period of 0500UTC-0700UTC 28 June 2023, term WPG was the most favorable factor accounting for the enhancement of KE (Fig. 9a), term HAK ranked second, and term VAK showed the least contribution. This indicates that, the strong winds were mainly produced, rather than horizontal or vertical transports.

Compared the zonal and meridional components of the horizontal transport (Sect. 2), it can be found that, the zonal component (i.e., HAK_U) mainly showed a favorable effect on the enhancement of strong winds within the key region (Fig. 9b), whereas, the meridional component (i.e., HAK_V) mainly decelerated the enhancement of

Fig. 9 Panel (**a**) shows the region averaged (within the box where the tripping incident of transmission line appeared) KE budget results (10^{-3} W kg^{-1}), where the thick grey dashed box marks the period when the tripping incident appeared, and the thin grey dashed line is the zero line. Panel (**b**) is the same as (a), but for the HAK associated with the zonal wind (HAK_U) and the HAK associated with the meridional wind (HAK_V). Panel (**c**) is the same as (a), but for the WPG associated with the zonal wind (WPG_U) and the WPG associated with the meridional wind (WPG_V)
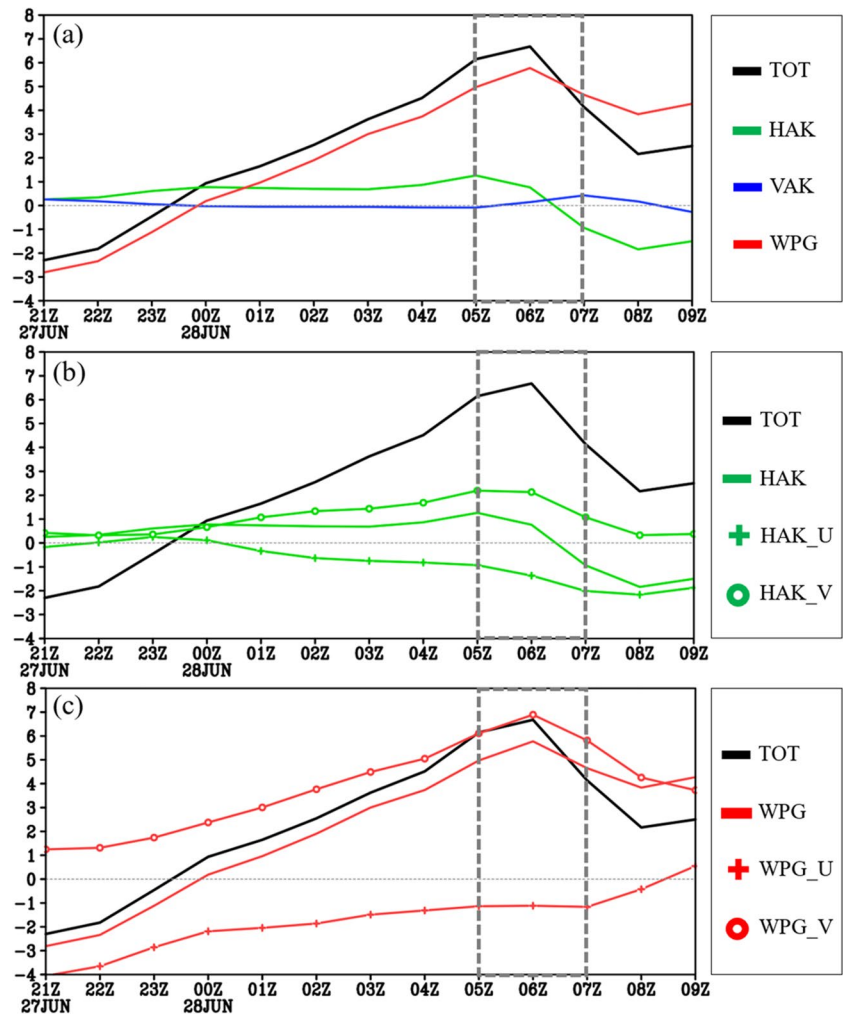
KE. Compared the zonal component with the meridional component of the WPG (Sect. 2), it is clear that, the meridional component (i.e., WPG_V) was the most favorable factor for the enhancement of wind within the key region. From Fig. 10, it can be seen that, there was a low center of geopotential height within the main body of the mesoscale vortex, whereas, in the regions south and east of the vortex, the geopotential height was higher than that associated with the vortex. This resulted in a nearly northward pointing pressure gradient force vector within the key region (Fig. 11). As a southwesterly wind dominated the key region (Fig. 10), the northward pressure gradient force did a positive work on the southwesterly wind, which caused the wind enhancement within this region. In contrast, the zonal component (i.e., WPG_U) mainly showed a negative effect, which decelerated the wind enhancement (Fig. 9c). This is mainly because that, the zonal component of the pressure gradient force was mainly pointing to the west (Fig. 11), because the center of the mesoscale vortex was mainly located to the northwest of the key region (Fig. 10). A westward pointing

pressure gradient force did negative work on the southwesterly wind within the key region, which was detrimental for the wind enhancement.

5 Conclusion and Discussion

As one of the largest power companies in the world, every year, the SGCC suffers serious natural disasters, with the meteorological disasters contributing the most. Of these, strong winds often induce windage yaw discharge of transmission lines and even toppling of transmission towers, which deserve in-depth researches. In this study, we focused on a strong wind event on 28 June 2023, during which a severe tripping incident of transmission line occurred in Eastern Inner Mongolia. Compared with similar previous studies that investigated the SGCC related disasters, the following three points should be highlighted: (i) the formation mechansims of the strong winds were explored by using the quantitative KE budgets; (ii) the formation mechanisms of a mesoscale vortex, that was
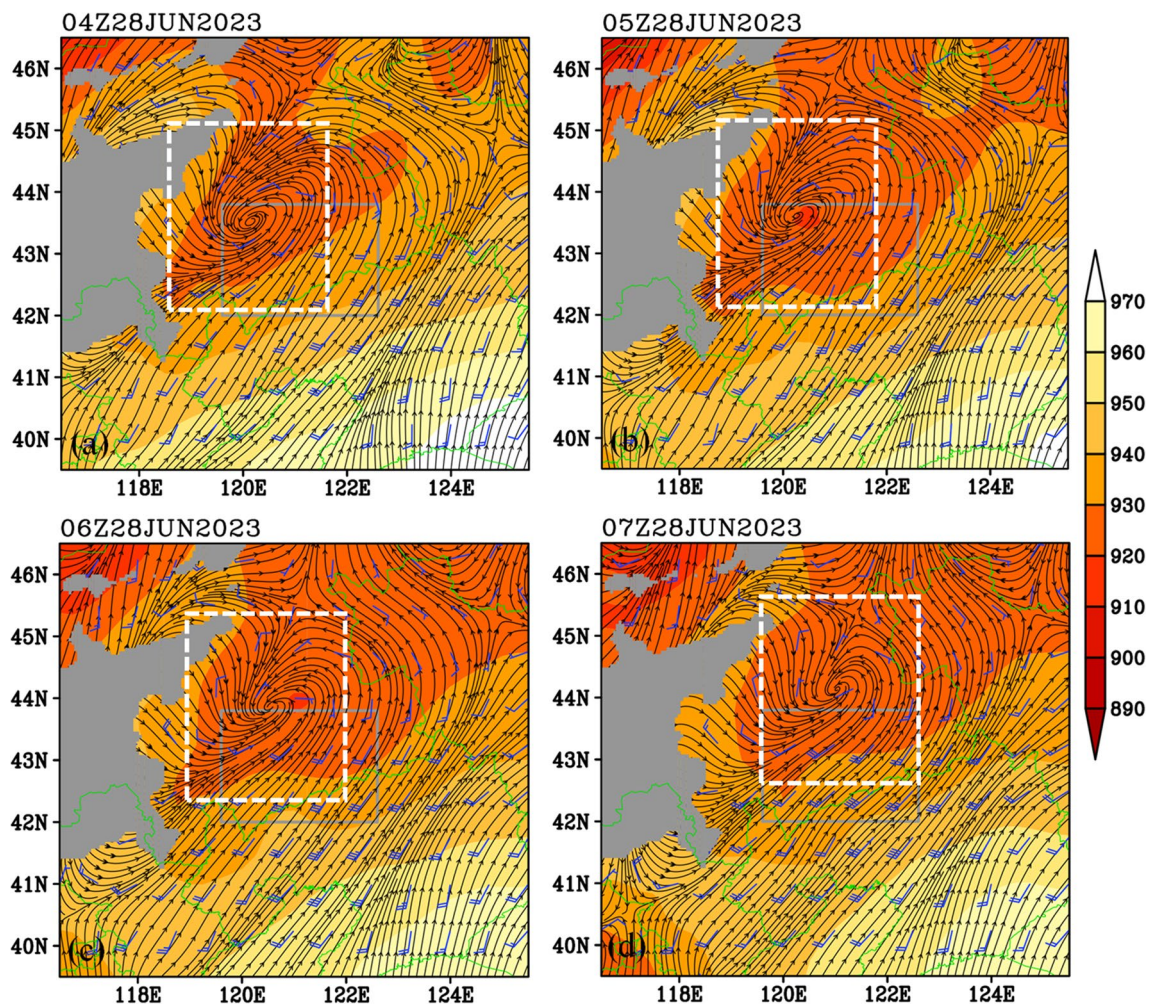
Fig. 10 Geopotential height (shading; gpm), stream field (black line with arrows), and wind (a full bar represents 4 m s^{-1}) at 900 hPa, where the grey box marks the location where the tripping incident of transmission line appeared, white dashed boxes outline the main body of the vortex, and the grey shading show the terrain above 1000 m

directly related to the strong winds, were clarified quantitatively through the vorticity budget; and (iii) the effects from the mesoscale vortex on the strong winds were shown by physical images. Related results are helpful to reach a more comprehensive understanding of such type of events.

Synoptic analysis shows that, the strong winds appeared under a favorable background environment, which was characterized by an intense upper-level divergence that was associated with a strong upper-level jet; and a strong middle-level warm advection that was ahead of a shortwave trough. In the lower troposphere, the most striking feature of the event was that a mesoscale vortex appeared, and maintained for a lifespan of ~19 h, with the strong winds mainly occurred in its southeastern quadrant. Vorticity budget indicates that the period from 2100 UTC 27 to 0100 UTC 28 June 2023 was the key stage for the formation of the mesoscale vortex, during which the cyclonic vorticity increased rapidly mainly due to the lower-level convergence-related vertical stretching. In

addition, as the convection developed, vertical transport of cyclonic vorticity acted as the second dominant factor for the vortex's formation. In contrast, tilting showed an overall neutral effect, and the horizontal transport mainly resulted in a net export of cyclonic vorticity, which acted as the most detrimental factor for the formation of the mesoscale vortex. Kinetic energy budget shows that, the most rapid wind enhancement appeared within the southeastern quadrant of the mesoscale vortex. Before the formation of the mesoscale vortex, the wind speed within its southeastern quadrant was decreasing, whereas, after the mesoscale-vortex's formation, the strong winds enhanced rapidly within this quadrant. Overall, the positive work done by the pressure gradient force was the most favorable factor accounting for the enhancement of strong winds; the horizontal transport ranked second, and the downward transport of KE (i.e., the downward momentum transportation) showed the least contribution. Further analyses show that, the positive work done by the northward pressure gradient
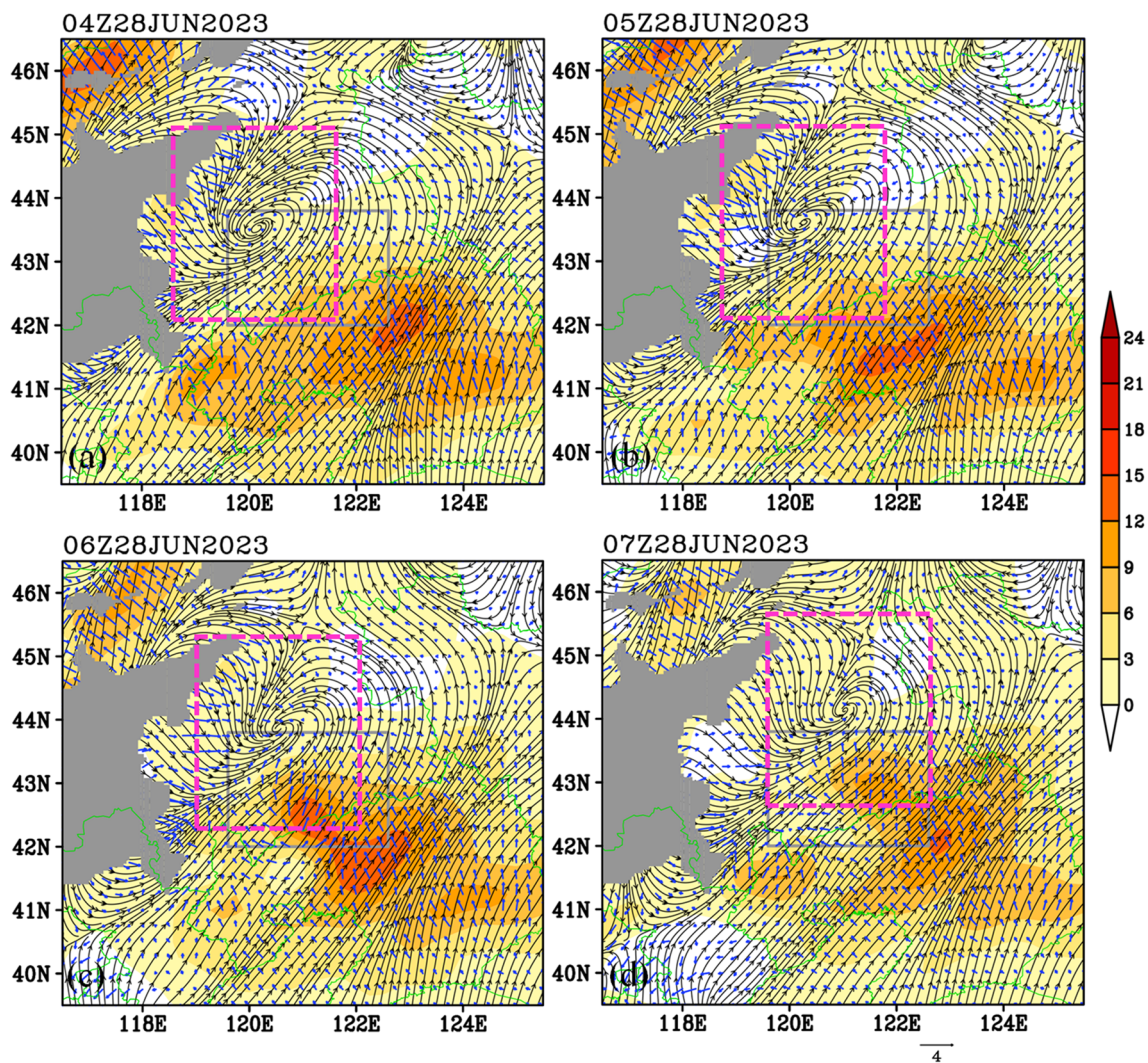
Fig. 11 The WPG associated with the meridional wind (shading; 10^{-3} W kg^{-1}), stream field (black line with arrows), and the pressure gradient force (vector; 10^{-3} m s^{-2}) at 900 hPa, where the grey box marks the location where the tripping incident of transmission line appeared, the purple dashed boxes outline the main body of the vortex, and the grey shading show the terrain above 1000 m

force (which was associated with the mesoscale vortex) on the southwesterly wind within the southeastern quadrant of the mesoscale vortex was the dominant factor for the enhancement of strong winds; and the zonal transport of KE was the second dominant factor. In contrast, the westward pointing pressure gradient force that was associated with the mesoscale vortex mainly did a negative work, and the meridional transport of KE mainly caused a net divergence, both of which were detrimental for the enhancement of the strong winds.

In this study, we provide the key mechanisms accounting for the occurrence of the strong winds that caused the tripping incident of transmission line in Eastern Inner Mongolia. Results indicate that, a lower-level mesoscale vortex was crucial for producing the disastrous strong winds. Therefore, improving the forecasts accuracy of lower-level mesoscale vortices (through finding the optimal configuration

of different physical schemes in the numerical model, using data assimilation for high-resolution meteorological observations, conducting corrections on numerical forecast results via deep learning, etc.) would be beneficial for improving the forecast accuracy of their associated strong winds. However, as a case study, its representativeness is limited (different types of background environments and different topography features all affect the final results). So, we suggest to conduct more studies on the strong winds in the future, which may reach a more comprehensive understanding of this type of event. Moreover, as high-resolution numerical simulations are useful for analyzing disaster weathers, we will conduct high-resolution simulations by using mesoscale models in the future. This is helpful to enhance the understanding of the formation of the strong winds associated with mesoscale vortices.

References

Cevik, H.H., Cunkas, M., Polat, K.: A new multistage short-term wind power forecast model using decomposition and artificial intelligence methods. Phys. A Stat. Mech. Appl. **534**, 122177 (2019)

Ding, J., Chen, Y., Wang, Y., Xu, X.: The southeasterly gale in Tianshan Grand Canyon in Xinjiang, China: a case study. J. Meteorol. Soc. Jpn **97**, 55–67 (2019)

Fu, S.-M., Yu, F., Wang, D.-H., Xia, R.-D.: A comparison of two kinds of eastward-moving mesoscale vortices during the mei-yu period of 2010. Sci. China Earth Sci. **56**(2), 282–300 (2013). https://doi.org/10.1007/s11430-012-4420-5

Fu, S.-M., Li, D.-S., Sun, J.-H., Si, D., Ling, J., Tian, F.-Y.: A 31-year trend of the hourly precipitation over South China and the associated mechanisms. Atmos. Sci. Lett. **17**, 216–222 (2016). https://doi.org/10.1002/asl.645

Fu, S.-M., Sun, J.-H., Luo, Y.-L., Zhang, Y.-C.: Formation of long-lived summertime mesoscale vortices over central east China: Semi-idealized simulations based on a 14-year vortex statistic. J. Atmos. Sci. **74**, 3955–3979 (2017)

Fu, S.-M., Mai, Z., Sun, J.-H., Li, W.-L., Ding, Y., Wang, Y.-Q.: Impacts of convective activity over the Tibetan Plateau on plateau vortex, southwest vortex, and downstream precipitation. J. Atmos. Sci. **76**, 3803–3830 (2019)

Fu, S.-M., Jin, S.-L., Shen, W., Li, D.-Y., Liu, B., Sun, J.-H.: A kinetic energy budget on the severe wind production that cause a serious state grid failure in Southern Xinjiang China. Atmos. Sci. Lett. **2020**, e977 (2020). https://doi.org/10.1002/asl.977

Fu, S.-M., Tang, H., Sun, J.-H., Zhao, T.-B., Li, W.-L.: Historical rankings and vortices' activities of the extreme Mei-yu seasons: Contrast 2020 to previous Mei-yu seasons. Geophys. Res. Lett. **49**, e2021GL096590 (2022). https://doi.org/10.1029/2021GL096590

Hersbach, H., Bell, B., Berrisford, P., et al.: The ERA5 global reanalysis. Quart. J. Roy. Meteor. Soc. **146**, 1999–2049 (2020)

Holton, J.R.: An introduction to dynamic meteorology, p. 552. Academic Press, San Diego (2004)

Huffman, G. J., Stocker, E. F., Bolvin, D. T., Nelkin, E. J., and Tan, J.: "GPM IMERG final precipitation L3 1 day 0.1 degree x 0.1 degree V06," in Goddard earth Sciences data and information services center. Editors Andrey Savtchenko and M. D. Greenbelt, **1**. https://www.re3data.org/repository/r3d100000036. (2019). https://doi.org/10.25504/FAIRsharing.7388wt . Accessed Jul 2023

Li, D.-S., Sun, J.-H., Fu, S.-M., Wei, J., Wang, S.-G., Tian, F.-Y.: Spatiotemporal characteristics of hourly precipitation over central eastern China during the warm season of 1982–2012. Int. J. Climatol. **36**, 3148–3160 (2016). https://doi.org/10.1002/joc.4543

Li, D., Liu, J., Liu, B., Fan, W., Yang, D., Xiao, X.: Simulation Analyses on a Downburst Event That Caused a Severe Tower Toppling down Accident in Zhejiang (China). Atmosphere **14**, 427 (2023). https://doi.org/10.3390/atmos14030427

Lu, B., Shi, Y.Q., Wang, G.H., Yue, B.: Numerical study of severe downslope winds at Kelamayi, XinJiang. Acta Meteor. Sin. **72**, 1218–1230 (2014)

Ma, H., Li, G.Q., Zeng, C.K., Wang, F., Jin, S.L., Fu, S.-M.: Evolutionary mechanisms of the strong winds associated with an intense cold wave event and their effects on the wind power production. Front. Earth Sci. **10**, 1054037 (2023). https://doi.org/10.3389/feart.2022.1054037

Markowski, P., Richardson, Y.: Mesoscale Meteorology in Midlatitudes, p. 407. Wiley-Blackwell, Hoboken, NJ (2010)

Song, H., Wu, Q., Li, H., Yin, W., Zhao, W.: Research on the application of meteorological disaster model in power grid transportation inspection business. J. Catastrophol. **4**, 68–72 (2019)

Sun, J., Ge, R., Zheng, L., Hu, C.: Analysis of state grid security operation in 2010. Electric Power **44**, 1–4 (2011)

Sun, J.-H., Zhang, Y.-C., Liu, R.-X., Fu, S.-M., Tian, F.-Y.: A review of research on warm-sector heavy rainfall in China. Adv. Atmos. Sci. **36**, 1299–1307 (2019)

Wang, C.H., Jin, S.L., Yang, S.L.: Simulation and analysis of the thermal-dynamics characteristics of "2.28" severe wind event in Xinjiang with WRF model. J. Desert Res. **31**, 511–516 (2011)

Xie, Q., Li, J.: Current situation of natural disaster in electric power system and counter measures. J. Nat. Disasters **15**, 126–131 (2006)

Yang, X.-L., Sun, J.-H.: The characteristics of cloud-toground lightning activity with severe thunderstorm wind in south and north China. Atmos. Ocean. Sci. Lett. **7**, 571–576 (2014)

Yang, J., Hao, Y., Chen, D., Jiang, B.: Relationship of power load and weather in agricultural region of Xinjiang. Meteorol. Monthly **35**, 114–118 (2009)

Zhang, B., Li, X., Wang, S.: A novel case adaptation method based on an improved integrated genetic algorithm for power grid wind disaster emergencies. Expert Syst. Appl. **42**, 7812–7824 (2015)

Zhang, G., Zhang, D., Sun, S.: On the orographically generated low-level easterly jet and severe downslope storms of March 2006 over the Tacheng Basin of Northwest China. Mon. Weather Rev. **146**, 1667–1683 (2018)

Zhang, Y., Yang, S., Guo, Z., Guo, Y., Zhao, J.: Wind speed forecasting based on wavelet decomposition and wavelet neural networks optimized by the Cuckoo search algorithm. Atmos. Ocean. Sci. Lett. **12**, 107–115 (2019)